



LAWRENCE  
LIVERMORE  
NATIONAL  
LABORATORY

LLNL-TR-667274  
CODT-2014-0794

# Thermal Analysis and Thermal Properties of ANPZ and DMDNP

**Elizabeth A. Glascoe, Heidi C. Turner, and Alexander E. Gash**

*Lawrence Livermore National Laboratory  
7000 East Avenue  
Livermore, CA 94550*

September 8, 2014

The work performed under the auspices of the U.S. Department of Energy by  
Lawrence Livermore National Laboratory under Contract DE-AC52-07NA27344.

## DISCLAIMER

This document was prepared as an account of work sponsored by an agency of the United States government. Neither the United States government nor Lawrence Livermore National Security, LLC, nor any of their employees makes any warranty, expressed or implied, or assumes any legal liability or responsibility for the accuracy, completeness, or usefulness of any information, apparatus, product, or process disclosed, or represents that its use would not infringe privately owned rights. Reference herein to any specific commercial product, process, or service by trade name, trademark, manufacturer, or otherwise does not necessarily constitute or imply its endorsement, recommendation, or favoring by the United States government or Lawrence Livermore National Security, LLC. The views and opinions of authors expressed herein do not necessarily state or reflect those of the United States government or Lawrence Livermore National Security, LLC, and shall not be used for advertising or product endorsement purposes.

## Introduction

The thermal properties of ANPZ and DNDMP are reported here. These properties were measured upon request for Pantex. The following is a list of the measurements requested:

- Density ( $\text{g}/\text{cm}^3$ )
- Decomposition Energy (Heat of Decomposition;  $\text{cal}/\text{g}$ )
- Pre-exponential factor (Arrhenius equation;  $1/\text{s}$ )
- Activation Energy (Arrhenius equation;  $\text{cal}/\text{mole}$ )
- Thermal Conductivity ( $\text{cal}/\text{cm}\cdot\text{s}\cdot\text{K}$ )

We have reported all most in SI units with the expectation that unit conversions can easily be performed by any individual reading this report. In many cases, we have provided more information than requested as it seemed relevant or necessary for performing safety calculations on these materials. The measurement methods and experimental details are described briefly in each section of this report.

## Density

ANPZ and DNDMP parts were die pressed for experiments with two 3-min dwells at 30,000 psi. The sample dimensions were measured using calipers (Mitutoyo IP65 coolant proof, 0.01mm resolution,  $\pm 0.02\text{mm}$  accuracy) and the mass was measured with a balance (Mettler Toledo AB2014-S, 0.1mg resolution, 0.1mg precision). Table T1 reports the sample dimensions and densities for several experimental parts.

**Table T1.** Sample dimensions and densities.

<b>ANPZ</b>		
<b>Sample Dimension (mm)</b>	<b>Ave Density (g/cc)</b>	<b>Sample application</b>
d = 6.315, h = 5.948	1.735	TMA Expts (3 samples)
d = 12.684, h = 3.137	1.750	Thermal Diffusivity Expts (3 samples)
<b>DNDMP</b>		
<b>Sample Dimension (mm)</b>	<b>Ave Density (g/cc)</b>	<b>Sample application</b>
d = 6.335, h = 5.883	1.532	TMA Expts (3 samples)
d = 12.719, h = 3.197	1.547	Thermal Diffusivity Expts (3 samples)

## Thermal Expansion

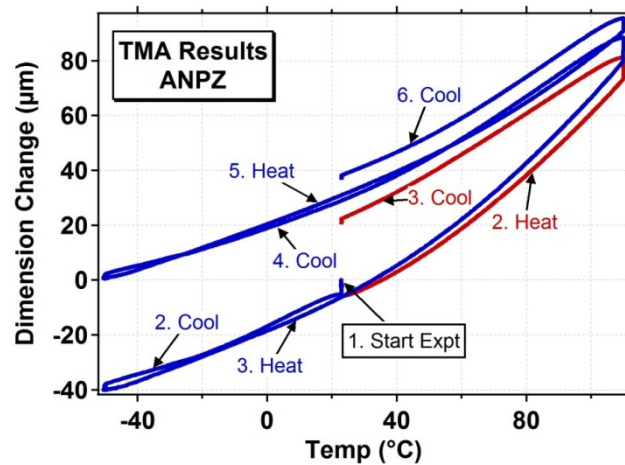
Thermal mechanical analysis experiments (TMA) were performed using a TA Instruments 2910 from  $-50$  to  $110$   $^{\circ}\text{C}$ . Samples were heated or cooled at approximately  $3$   $^{\circ}\text{C}/\text{min}$  for one or multiple cycles. Sample dimensions and density are reported in Table T1.

Figure F1 shows the results of two different ANPZ experiments, using a pristine part in each experiment. The figure demonstrates the expansion/contraction of the material as it is cooled or heated. The blue curve shows the first experiment. The overlap of the cooling ("2. Cool") and heating ("3. Heat") curves in the sub-ambient stage indicates a reversible response. Heating the sample to the higher

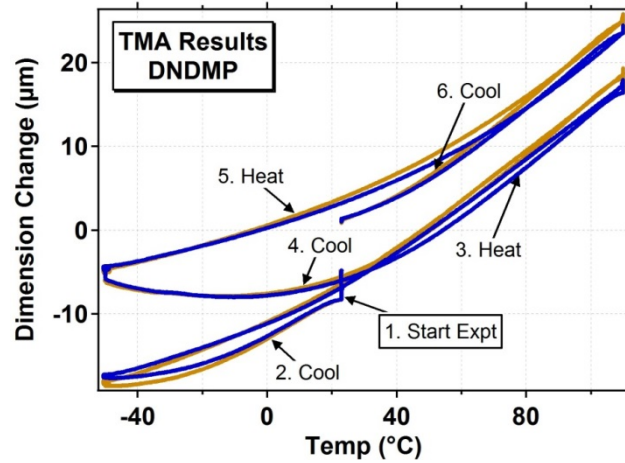
temperatures causes an irreversible expansion as indicated by the disparity between the heating stage (“3. Heat” ) and the cooling stage (“4. Cool”) of the blue curve. The material shows additional expansion after the second high temperature excursion (i.e. “5. Heat” versus “6. Cool”). A second sample (red curve) was heated and cooled above the room temperature and shows excellent overlap with the first sample (blue curve).

Figure F2 shows the results for two different DNDMP pressed parts during several heat/cool cycles. The overlap of the two experiments (blue curve vs. brown curve) demonstrates the reproducibility of the results. In general, one can see that the first cooling step (“2. Cool”) overlaps well with the first heating step (“3. Heat”). The second cooling stage (“4. Cool”) has excellent overlap with prior heating (“3. Heat”) but shows sudden divergence in the sub-ambient region. The reproducibility of this phenomenon in three different experiments/samples (only two shown here) indicates that this is not an artifact or anomaly. Characterizing the irreversible dimensional changes in this sample is beyond the scope of this report but should be explored further.

These data were used in conjunction with thermal diffusivity and heat capacity measurements to calculate thermal conductivity. In the thermal diffusivity experiments, the sample was cooled to -50 °C and stepped up to 110 °C. We chose to use the first -50 to 110 °C scan from the TMA experiments because the conditions most closely matched the thermal diffusivity experiments. The data were fit to polynomials and the  $dL/L_0$  values were used in the NETZSCH thermal diffusivity software in order to calculate density as a function of temperature. Table T2 lists the polynomial, dimension changes and  $dL/L_0$  values used in the thermal diffusivity software.



**Figure F1.** Thermal mechanical analysis experimental results for two different ANPZ pressed parts.



**Figure F2.** Thermal mechanical analysis experimental results for two different DNDMP pressed parts.

**Table T2.** Dimension change ( $dL$ ) and relative dimension change ( $dL/L_0$ ) used to calculate thermal conductivity.

	ANPZ Polynomial: $dL = 0.0033T^2 + 0.5212T - 13.96$ $L_0 = 5.9604$ mm		DNDMP Polynomial: $dL = 0.0008T^2 + 0.186T - 12.032$ $L_0 = 5.9219$ mm	
Temp (°C)	Dimension change, $dL$ (µm)	Relative dimension change, $dL/L_0$ (m/m)	Dimension change, $dL$ (µm)	Relative dimension change, $dL/L_0$ (m/m)
-65	-33.8955	-5.6868E-03	-20.7420	-3.5026E-03
-55	-32.6435	-5.4767E-03	-19.8420	-3.3506E-03
-45	-30.7315	-5.1559E-03	-18.7820	-3.1716E-03
-35	-28.1595	-4.7244E-03	-17.5620	-2.9656E-03
-25	-24.9275	-4.1822E-03	-16.1820	-2.7326E-03
-15	-21.0355	-3.5292E-03	-14.6420	-2.4725E-03
-5	-16.4835	-2.7655E-03	-12.9420	-2.1854E-03
5	-11.2715	-1.8911E-03	-11.0820	-1.8714E-03
15	-5.3995	-9.0590E-04	-9.0620	-1.5303E-03
25	1.1325	1.9000E-04	-6.8820	-1.1621E-03
35	8.3245	1.3966E-03	-4.5420	-7.6698E-04
45	16.1765	2.7140E-03	-2.0420	-3.4482E-04
55	24.6885	4.1421E-03	0.6180	1.0436E-04
65	33.8605	5.6809E-03	3.4380	5.8056E-04
75	43.6925	7.3305E-03	6.4180	1.0838E-03
85	54.1845	9.0907E-03	9.5580	1.6140E-03
95	65.3365	1.0962E-02	12.8580	2.1713E-03
105	77.1485	1.2944E-02	16.3180	2.7555E-03
115	89.6205	1.5036E-02	19.9380	3.3668E-03
125	102.7525	1.7239E-02	23.7180	4.0051E-03

## Heat Capacity

Measurements of the heat capacity of ANPZ and DNDMP are underway; however, instrument challenges and delays have necessitated generating a set of “best guess” values for the heat capacity. The heat capacity values are used to calculate the thermal conductivity in the next section. Our thermal properties database contains several heat capacity measurements for various explosives. All measurements were performed using a TA Instruments M2920 DSC. Figure F3 shows the heat capacity for several different explosives; all the explosives have similar heat capacities, probably because they are all CHNO based molecules with similar bonds. We chose to use the RX-55-AE data as a best guess for the ANPZ and DNDMP heat capacity because it spans the most extreme range of heat capacities and because LLM-105 is structurally similar to ANPZ and DNDMP. The RX-55-AE heat capacity was measured between -50 and 120 °C, fit to a polynomial, and additional values at -55 and 125 °C were calculated from the polynomial. The polynomial is reported in Figure F3; Table T3 lists the heat capacity values for RX-55-AE.

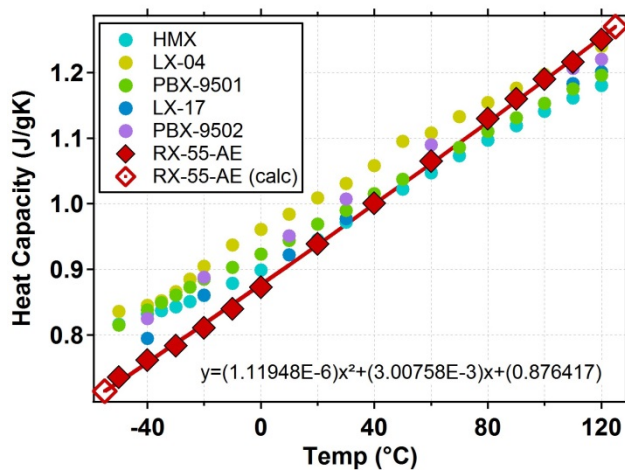


**Figure F3.** Heat capacity measurements for explosives and explosive formulations. LX-04 is 85% HMX and 15% Viton A; PBX-9501 is 95% HMX, 2.5% Estane, and 2.5% BDNPA/F; LX-17 is 92.5% TATB and 7.5% Kel-F 800; PBX-9502 is 95% TATB and 5% Kel-F 800; RX-55-AE is 97.5% LLM-105 and 2.5% Viton A. The RX-55-AE data between -50 and 120 °C were fit to a polynomial; the data points at -55 and 125 °C were calculated using the polynomial.

**Table T3.** Heat capacity values for RX-55-AE (97.5% LLM-105 and 2.5% Viton A). These values were used to calculate the thermal conductivity in the next section.

Temp (°C)	C <sub>p</sub> (J/gK)
-55	0.714387 (calc)
-50	0.736
-40	0.762
-30	0.784
-20	0.811
-10	0.840
0	0.873
20	0.939
40	1.001
60	1.065
80	1.130
90	1.160
100	1.190
110	1.216
120	1.250
125	1.269856 (calc)

### Thermal Conductivity and Thermal Diffusivity

The thermal diffusivity of ANPZ and DNDMP were measured at multiple temperatures using the Netzsch LFA 457. Transient thermal diffusivity is measured by rapidly heating one surface of a material with a 300 microsecond pulse of near-IR laser light (typically 1-5 J/pulse) and measuring the heat evolved from the opposite surface with a cryogenically cooled Mercury-Cadimium-Tellurium (MCT) detector. The instrument is capable of measuring the thermal diffusivity of samples at static temperatures between -100 and 600 °C in a gas or vacuum environment; in these experiments the temperature was restricted to -50 and 120 °C for safety reasons . Helium gas was used for all experiments. The sample dimensions are reported in Table T1. All samples were spray-coated with graphite, and mounted into the instrument with a silicon-carbide (SiC) centering cone and SiC lid. Standard solid porcelain samples were tested using standard methods to ensure proper instrument operation; results of these tests indicate that the instrument is running within specifications (see Figure F4).

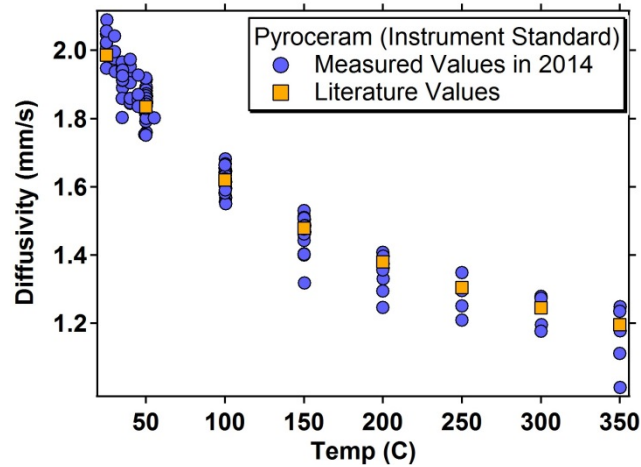


**Figure F4.** Thermal diffusivity of Pyroceram, a ceramic standard used for instrument validation.

Thermal diffusivity measurements on ANPZ and DNDMP are shown in Figure F5. Shot-to-shot variability is common, as can be seen in Figure F5, therefore diffusivity is measured many times at each temperature; a liner fit to the full data set is included in the figure. The mean value and standard deviation at each temperature are also plotted in Figure F5 and reported in Table T4. Measurements of thermal diffusivity were repeated for multiple samples and several shots at 30 °C were collected at the beginning and end of every experimental series in order to ensure that the sample was not altered by heating or cooling.

Thermal conductivity values were calculated using equation 1:

$$k = \alpha \rho C_p \quad (1)$$

Where  $k$  is thermal conductivity,  $\alpha$  is thermal diffusivity,  $\rho$  is density and  $C_p$  is heat capacity. The calculations were performed using the Netzsch software. The heat capacity values for RX-55-AE were used (see Table T3) and the thermal expansion values (Table T2) were used by the software to determine density ( $\rho$ ). The thermal conductivity values for both ANPZ and DNDMP are reported in Table T4 and plotted in Figure F6.

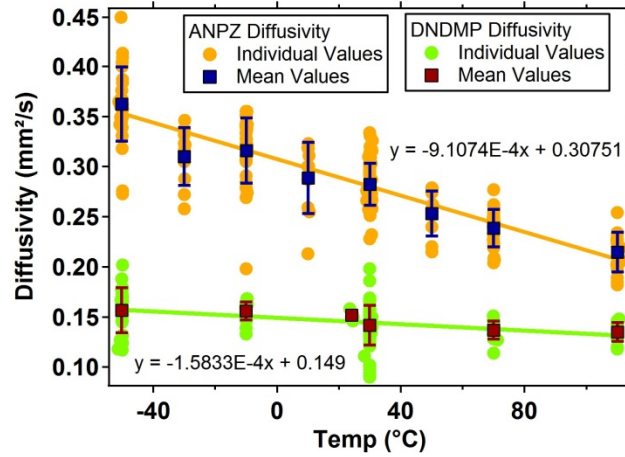


Figure F5. Measured thermal diffusivity for ANPZ and DNDMP.

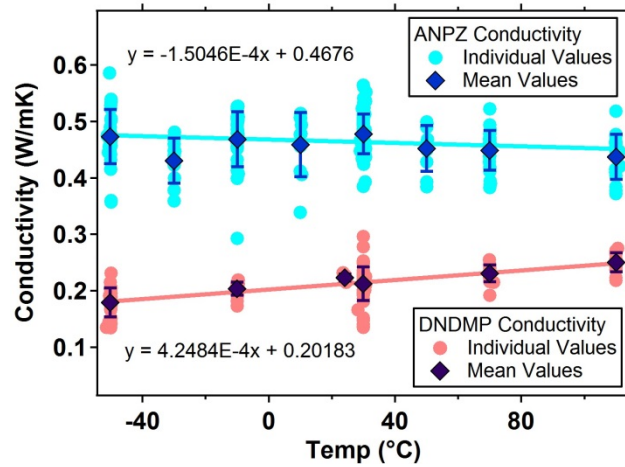


Figure F6. Thermal conductivity values for ANPZ and DNDMP; values were calculated using the heat capacity values for RX-55-AE.

**Table T4.** Mean thermal diffusivity and conductivity values for ANPZ and DNDMP. Conductivity values were calculated using the heat capacity values for RX-55-AE.

	Temp. (°C)	Diffusivity (mm <sup>2</sup> /s)	Conductivity (W/mK)	# of shots
ANPZ	-50.2 ± 0.3	0.36 ± 0.04	0.47 ± 0.05	30
	-29.9 ± 0.1	0.31 ± 0.03	0.43 ± 0.04	10
	-9.9 ± 0.1	0.32 ± 0.03	0.47 ± 0.05	30
	10.1 ± 0.1	0.29 ± 0.03	0.46 ± 0.06	10
	30.0 ± 0.3	0.28 ± 0.02	0.48 ± 0.04	80
	50.1 ± 0.1	0.25 ± 0.02	0.45 ± 0.04	10
	70.0 ± 0.1	0.24 ± 0.02	0.45 ± 0.04	26
	110.1 ± 0.4	0.21 ± 0.02	0.44 ± 0.04	20
DNDMP	-50.2 ± 0.3	0.16 ± 0.02	0.18 ± 0.03	23
	-10.0 ± 0.1	0.16 ± 0.01	0.20 ± 0.01	21
	24.2 ± 0.4	0.152 ± 0.004	0.22 ± 0.01	6
	30.0 ± 0.3	0.14 ± 0.02	0.21 ± 0.03	67
	70.1 ± 0.3	0.14 ± 0.01	0.23 ± 0.01	17
	110.0 ± 0.1	0.13 ± 0.01	0.25 ± 0.02	16

### Decomposition and Thermal Transitions

Differential scanning calorimetry (DSC) experiments were performed at multiple heating rates in order to characterize and quantify the thermal transitions, decomposition energy and decomposition kinetics. Pinhole pans were used for all DSC experiments. Figure F7 shows the DSC curves for ANPZ. At 10 °C/min there is one prominent peak at 358 °C. At 3, 1, and 0.3 °C/min there are two peaks; the first is a fairly smooth peak followed by an extremely sharp peak. The signal amplitude at 0.1 °C/min is too small to distinguish a peak in this plot but upon close inspection one can see a small peak; this data was excluded from the decomposition energy and kinetic analysis because of low signal amplitude. The 10 °C/min data were excluded from the decomposition energy and kinetic analysis because the heat flow rate was too high for the DSC instrument to resolve.

Figure F8 shows the DSC results for DNDMP at multiple heating rates. There is a prominent endotherm in all the experiments at 163 °C, which is indicative of a phase change. Further work is necessary to establish the nature of this phase change (i.e. melt, polymorph change, etc). A single exotherm is observed at all heating rates. The 10 °C/min data were excluded from the decomposition energy and kinetic analysis because of concerns that the heat flow rate was too high for the DSC instrument to resolve.

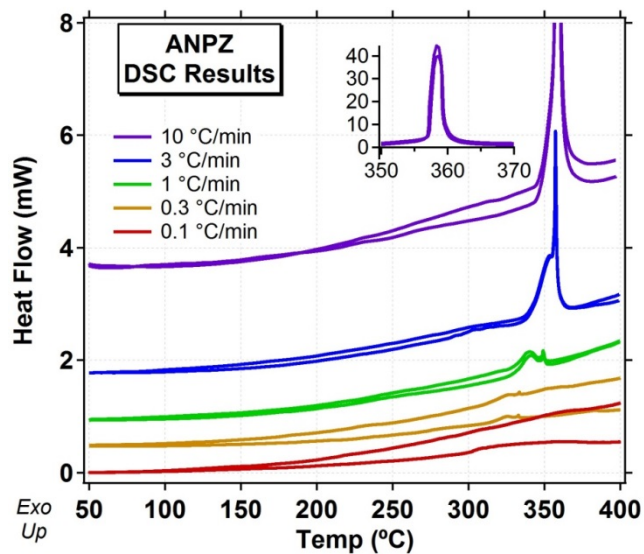


**Figure F7.** DSC results for ANPZ at multiple heating rates. The inset shows the full decomposition curve at 10 °C/min. These curves were shifted vertically for better visualization.

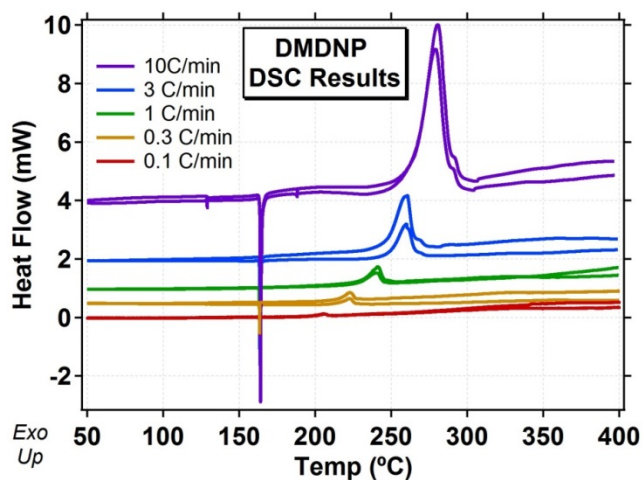


**Figure F8.** DSC results for DNDMP at multiple heating rates. These curves were shifted vertically for better visualization.

### Decomposition Energy

Decomposition energy was determined by integrating the heat-flow signal from the DSC curves; the results are reported in Table T5.

**Table T5. Heat-flow from DSC experiments on ANPZ and DNDMP using a pinhole pan.**

Heating rate (K/min)	ANPZ Heat-flow (J/g)	DNDMP Heat-flow (J/g)
0.1	na	-1201.2
0.1	na	-1307.3
0.3	-443.9	-1323.5
0.3	-503.1	-1421.1
1	-606.6	-990.4
1	-511.6	-1213.2
3	-864.6	-995.2
3	-792.9	-1514.7
AVERAGE	-620.5 +/- 171.1	-1245.8 +/- 186.7

## Kinetic Parameters

### *Kinetic Experiments and Modeling Methods*

The kinetic parameters were derived by modeling DSC experiments. In the experiments, the sample was decomposed in a pinhole pan at multiple heating rates and the heat-flow signals were used to parameterize the models. Three different methods were used to extract kinetic parameters; in all three methods the rate equation for fraction reacted begins with:

$$\frac{d\alpha}{dt} = kf(\alpha) = Ae^{-E/RT}f(\alpha) \tag{1}$$

where  $\alpha$  is fraction reacted (0-1),  $t$  is time,  $k$  is the Arrhenius rate constant,  $A$  is the pre-exponential factor,  $E$  is the activation energy,  $R$  is the gas constant,  $T$  is temperature, and  $f(\alpha)$  is the reaction model.

1. In the ASTM E698-11 method, we plot the log10 of the inverse heating rate,  $\log_{10}(1/\beta)$ , versus inverse peak-temperature ( $1/T_{\text{peak}}$ ) in order to calculate  $E$  and  $A$ . No corrections for heating rate or thermal correction were applied in the calculations here because the heating rate correction was out of range of the correction factors provided in the ASTM and, in the case of ANPZ, the double peak made it difficult to extract a precise peak height for each peak. The value for  $E$  was refined until it converged (in every case,  $E$  was refined twice to reach convergence). In all calculations, the temperature chosen for the  $E$  refinement was derived from 1 °C/min results.

This method is the simplest method, and there are a number of implied assumptions.

- Arrhenius behavior and first order reaction model, i.e.,  $\frac{d\alpha}{dt} = Ae^{-\frac{E}{RT}}(1 - \alpha)$
- Extent of reaction at the peak is constant and independent of heating rate

At LLNL we prefer to use more sophisticated methods such as isoconversional or extended prout-tompkins models for our thermal explosion predictions.

2. The second method is the Friedman isoconversional method, {Friedman, 1964 #125}, equation (1) is rearranged to the following:

$$\ln\left(\frac{d\alpha}{dt}\right) = \frac{-E_\alpha}{RT_\alpha} + \ln[A_\alpha f(\alpha)] \quad (2)$$

By plotting  $\ln(d\alpha/dt)$  versus  $1/T_\alpha$  (i.e. the temperature at each fraction point,  $\alpha$ , and fitting the data to a straight line, the values for  $E_\alpha$  and  $\ln\{A_\alpha f(\alpha)\}$  can be calculated. These values are dependent on the extent of the reaction. Typically the first and last 10% of the reaction are erroneous due to small signal-to-noise ratios of the data.

This method is a rigorous analysis method, however, the data can be hard to transfer because instead of a single A/E one has a table or plot of all  $E_\alpha$  values and corresponding  $\ln\{A_\alpha f(\alpha)\}$ . In general, this method is used as a cross check of the parameters derived from method 3.

3. The extended-Prout-Tompkins (e-PT) model is a nucleation and growth, global-kinetic-model {Burnham, 1999 #55; Burnham, 2007 #64}; the e-PT model is shown in equation 3:

$$\frac{d\alpha}{dt} = (Ae^{-E/RT})(1 - \alpha)^n(1 - q(1 - \alpha))^m \quad (3)$$

where  $\alpha$  is the fraction reacted,  $E$  is the activation energy,  $R$  is the gas constant,  $T$  is temperature,  $A$  is the pre-exponential factor, and  $n$ ,  $m$ , and  $q$  are unitless variables associated with the reaction order, autocatalysis and nucleation, respectively. The e-PT model is appropriate for modeling the kinetics of autocatalytic decomposition and is used to model many energetic material decompositions {Brill, 1994 #21; Behrens Jr., 1998 #106}.

In this method, full DSC decomposition curves are used to derive the kinetic parameters and therefore this method takes into account early decomposition processes which are the most relevant to thermal explosion calculations. This is the preferred method at LLNL for predicting thermal explosions.

### **ANPZ kinetic models**

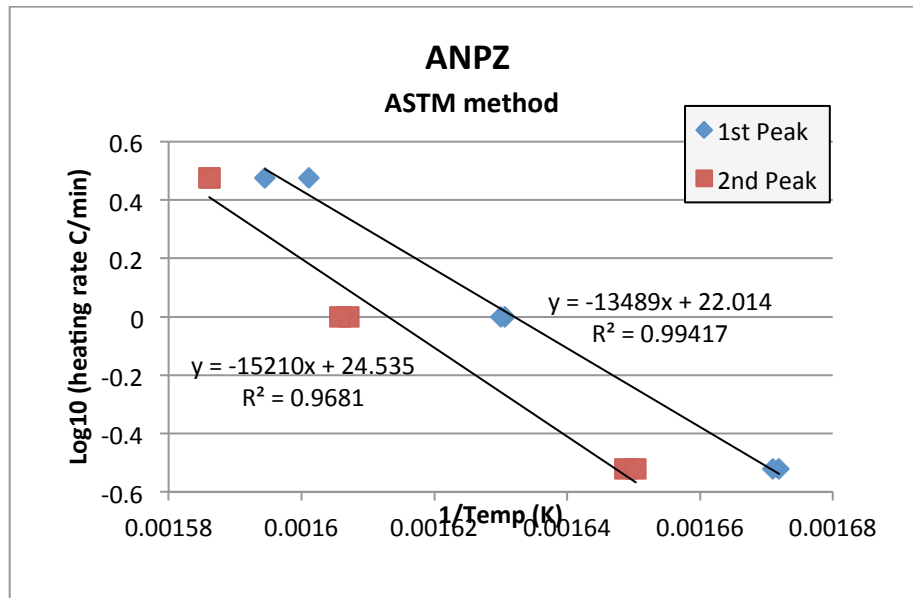
The ANPZ kinetics were difficult to resolve because there were two peaks in the DSC experiments. Figure F10 and F12 show the DSC data and one can see that the first peak is much broader than the second. We have analyzed both peaks and the results are summarized in Table T6. However, for time-to-explosion calculations, one can probably just use peak 1 as the material will most likely explode after only a few percent decomposition has been achieved (See Appendix for further verification of this recommendation). In general, the activation energy for the first peak is similar in all three methods, which increases our confidence in the accuracy of these analyses methods.

Figure F9 shows the ASTM analysis. Figure F10 shows a comparison of the DSC data with predictions using the ePT model. In the ePT analysis, only three heating rates were used, the slowest (0.1 °C/min) and fastest (10 °C/min) were poor quality and made it impossible to fit the data. One can see that the ePT model predictions match the data quite well for the first peak but the match is terrible for the second. No amount of tweaking could improve this fit.

Figure F11 shows the isoconversional analysis on the data. One can see that the first peak has an activation energy of ~60 kcal/mol and the second peaks out at ~110 kcal/mol. Figure F12 shows the DSC data with predictions from the isoconversional analysis; again, the predictions for the second peak show a poor match with experimental data.

**Table T6. ANPZ decomposition kinetic results**

Peak 1	Method	A (1/s)	E (kcal/mol)	Other parameters
	ASTM E698	1.7648E+18	59.279	NA
	Isoconv.		55.7427 (average value between $\alpha = 0.2$ and 0.6)	NA
	ePT	2.2397E+18	58.070	m = 0.73722 n = 0.89666 q = 0.99 f = 0.8
Peak 2	Method	A (1/s)	E (kcal/mol)	Other parameters
	ASTM E698	5.3548E+20	67.091	NA
	Isoconv.		79.030 (average value between $\alpha = 0.6$ and 0.95)	NA
	ePT	6.0034E+18	56.873	m = 1.7280 n = 2.8226 q = 0.99 f = 0.2



**Figure F9.** Plot of  $\log_{10}(\beta)$  vs.  $(1/T_{\text{peak}})$  used to extract A & E for ANPZ decomposition using ASTM E698 method

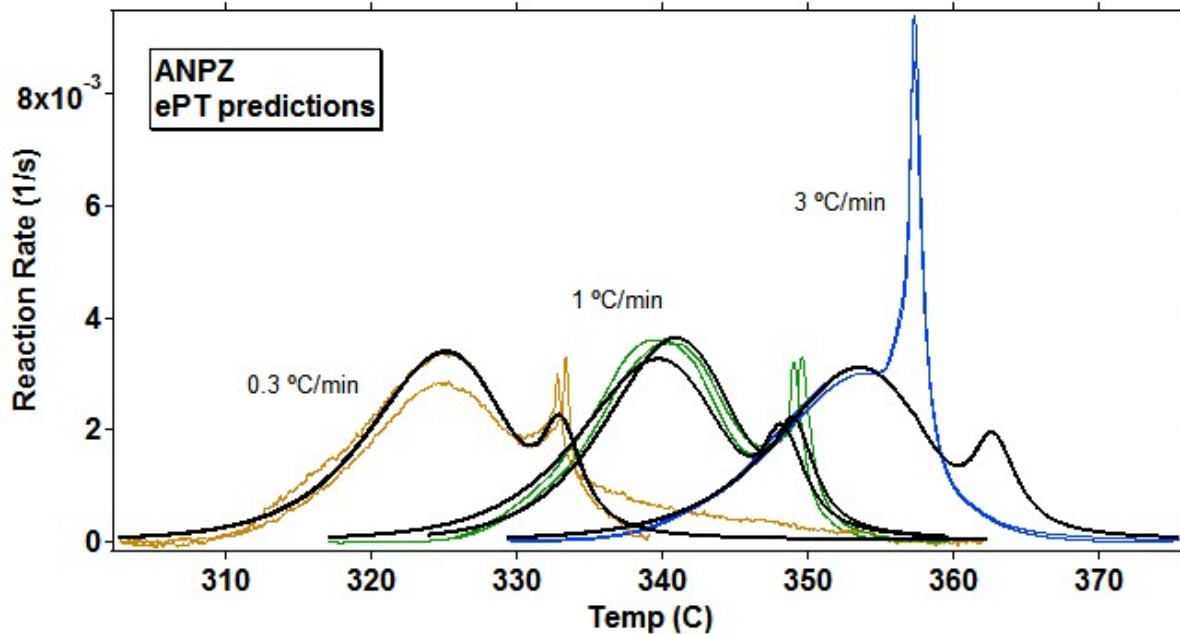


**Figure F10.** ANPZ exothermic DSC data (colored lines) with ePT model predictions (black lines). The reaction rate data and predictions at 0.3 and 1 °C/min were amplified (x10, x3 respectively) for better visualization in this figure.

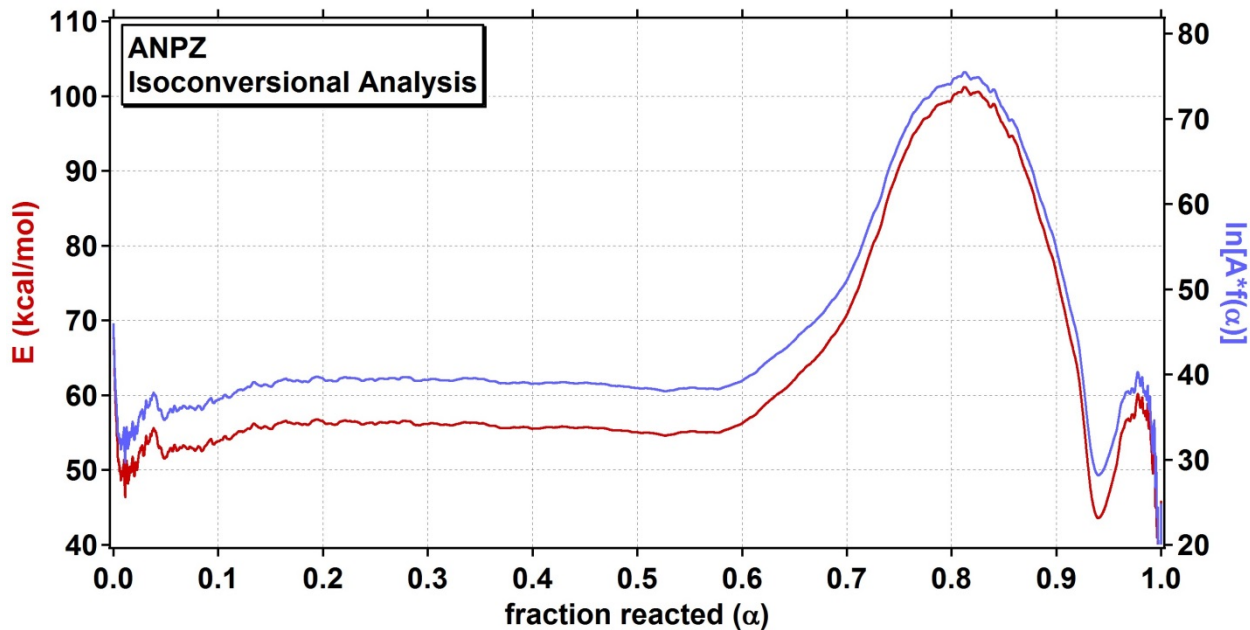


**Figure F11.** ANPZ isoconversional analysis results. Note,  $\alpha = 0.6$  corresponds to ca. 355 °C on the 3C/min curve in Figure F12, which is the point in the DSC curve where the reaction rate and heat flow rise quickly. .

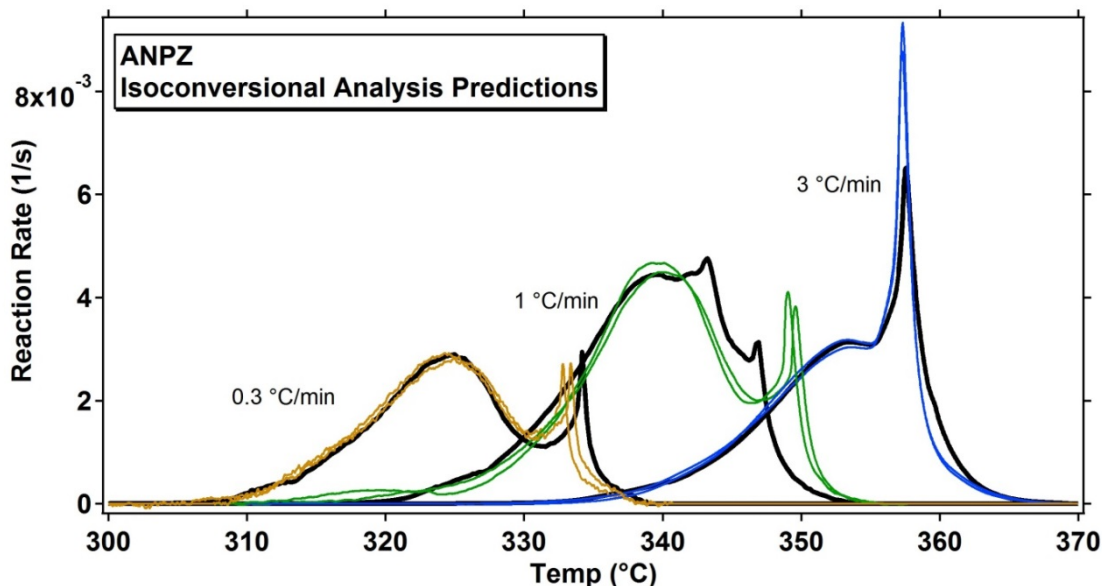


**Figure F12.** ANPZ exothermic DSC data (colored lines) with isoconversional analysis predictions (black lines). The reaction rate data and predictions at 0.3 and 1 °C/min were amplified (x8, x4 respectively) for better visualization in this figure.

### ***DNDMP Kinetic models***

The DNDMP kinetics were much easier to analyze because the DSC data showed a single smooth decomposition curve (see Fig. F14 or F16). The analysis results are summarized in Table T7. All three methods produce similar activation energies, which increases our confidence in the accuracy of these analyses methods.

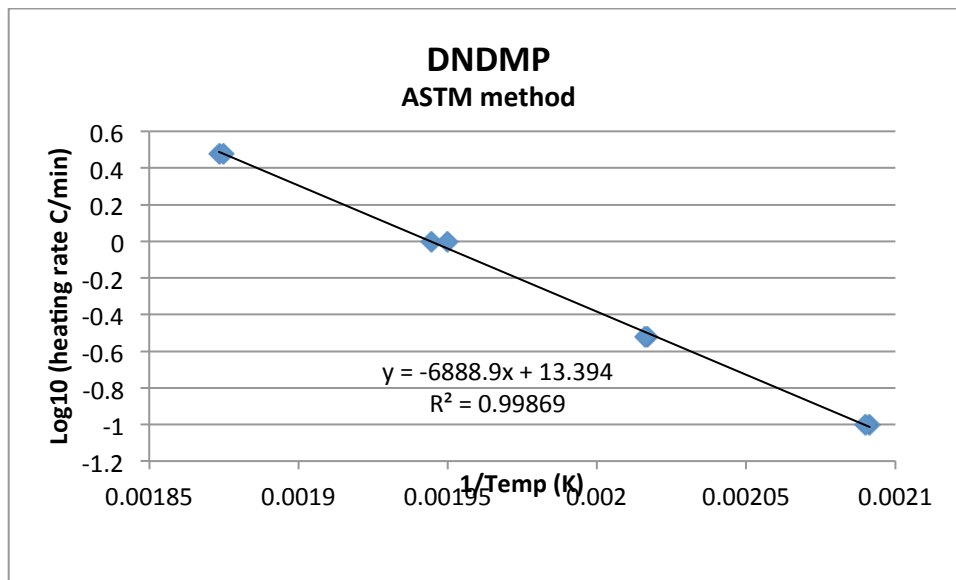
Figure F13 shows the ASTM analysis. Figure F14 shows a comparison of the DSC data with predictions using the ePT model. One can see that the ePT model predictions match the data quite well at all the heating rates.

Figure F15 shows the isoconversional analysis on the data. One can see that the material has an activation energy of ~28 kcal/mol over most of the decomposition range. Figure F16 shows the DSC data with predictions from the isoconversional analysis; the predictions show excellent match with experimental data.

**Table T7. DNDMP decomposition kinetic results**

<i>Method</i>	<i>A (1/s)</i>	<i>E (kcal/mol)</i>	<i>Other parameters</i>
ASTM E698	3.1414E+9	29.473	NA
Isoconv.	NA	28.8 (average value between $\alpha = 0.2$ and $0.8$ )	NA
ePT	2.0806E+10	29.554	$m = 0.95833$ $n = 0.96352$ $q = 0.99$

**ASTM E698**



**Figure F13.** Plot of  $\ln(1/\beta)$  vs.  $(1/T_{peak})$  used to extract A & E for DNDMP decomposition using ASTM E398 method

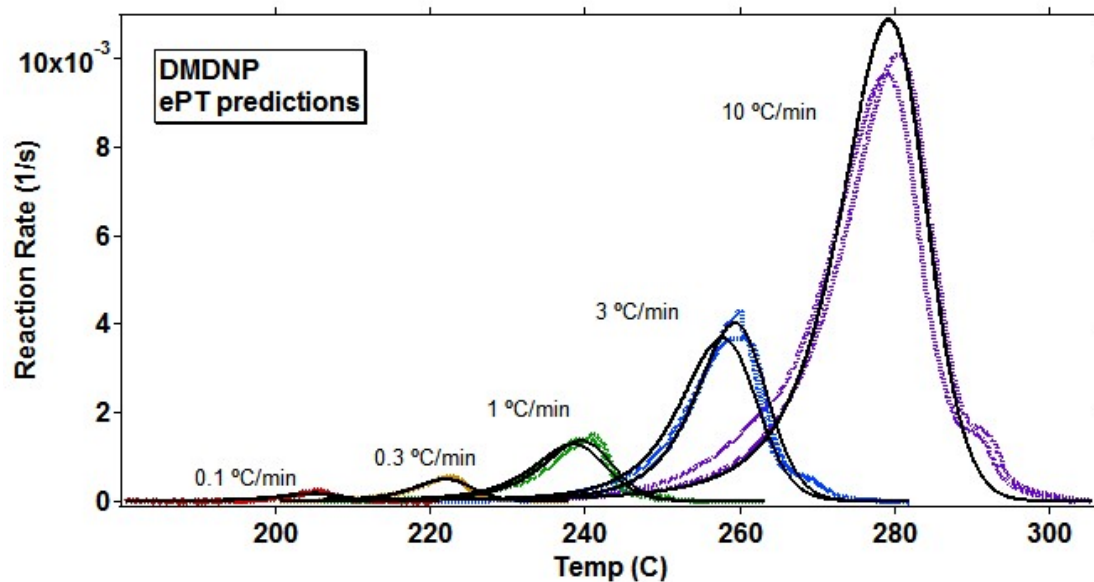


Figure F14. DNDMP exothermic DSC data (colored lines) with ePT model predictions (black lines).

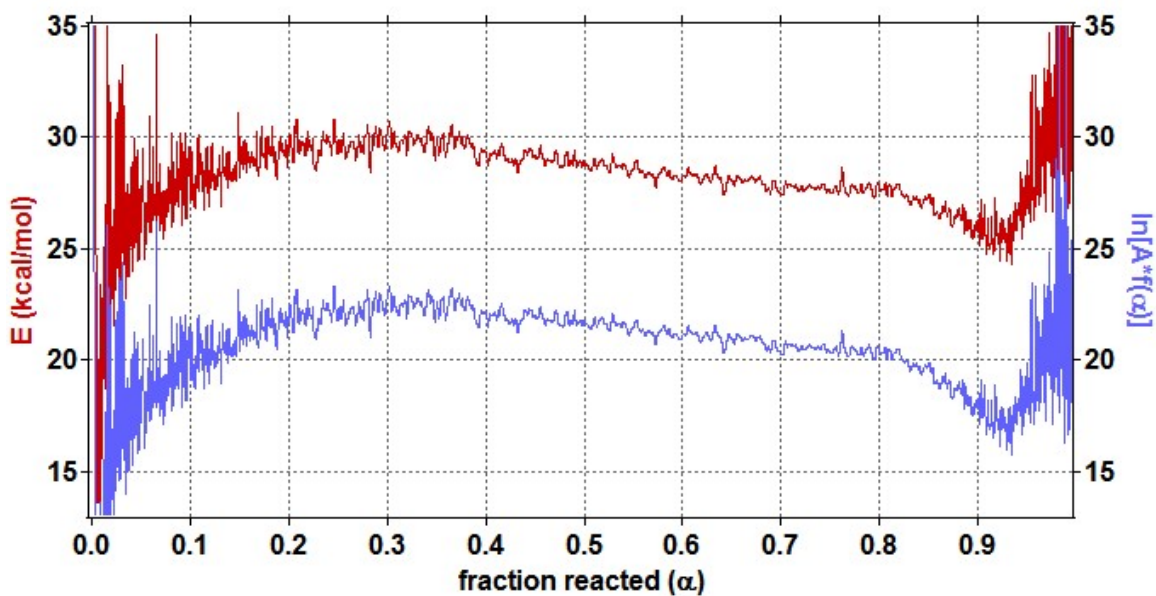


Figure F15. DNDMP isoconversional analysis results.

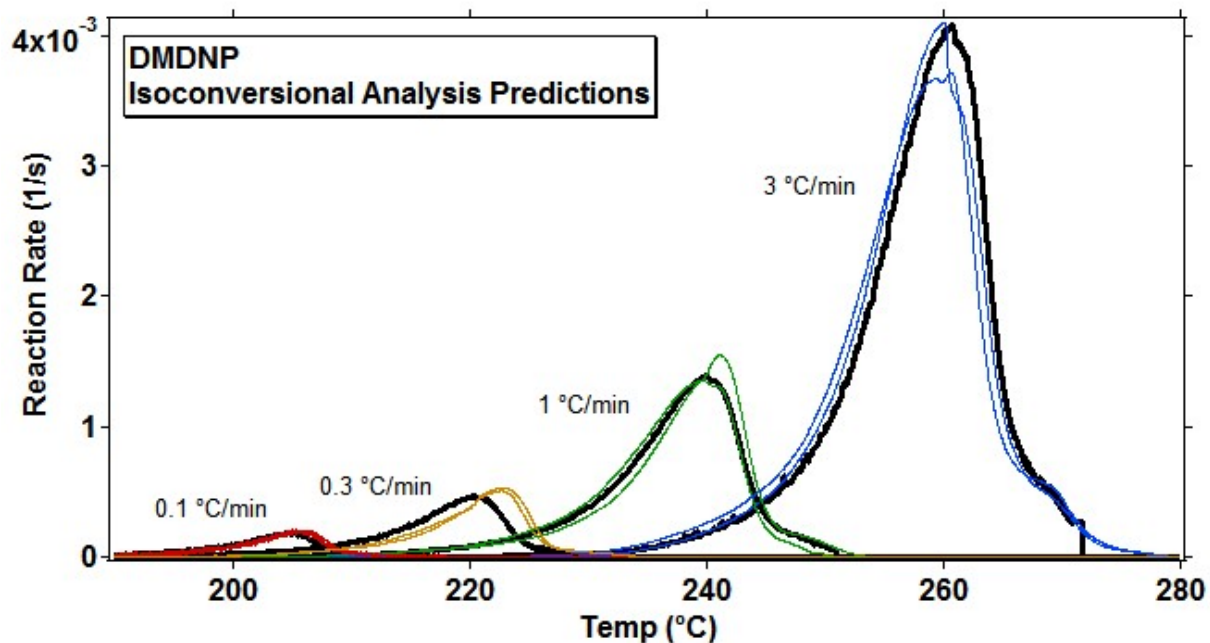


Figure F16. DNDMP exothermic DSC data (colored lines) with isoconversional analysis predictions (black lines).

## Appendix

### A1. ASTM calculation details

The following data is provided for users to do further ASTM calculations if desired. These values are uncorrected and derived directly from the DSC data. The Q2000 DSC used for these experiments is a heat flux DSC.

ANPZ				DNDMP		
DSC File number	Heating Rate (°C/min)	1st peak temp (°C)	2nd peak temp (°C)	DSC File number	Heating Rate (°C/min)	peak temp (°C)
Q13-774.001	0.3	324.97	333.38	Q14-063	0.1	205
Q13-770	0.3	325.31	332.79	Q14-043	0.1	205.32
Q13-769	1	340.13	349.06	Q14-042	0.3	222.67
Q13-772	1	340.37	349.6	Q14-064	0.3	222.85
Q13-768	3	351.42	357.27	Q14-052	1	241.09
Q13-773.001	3	354	357.32	Q14-050	1	239.66
				Q14-051	3	260.65
				Q14-049	3	260.17

### A2. Time to Maximum Reaction Rate under Adiabatic Conditions (TMRad)

It is often times helpful to compare the different kinetic models based on a prediction rather than the kinetic parameters, especially since the models are different making it unreasonable to directly compare parameters. Here we have performed the simplest prediction one can do with a kinetic model: calculating the time to maximum reaction rate under adiabatic conditions (TMRad) using the AKTS software. This calculation is an isothermal calculation (temperature defined by the user) with an adiabatic condition so that all heat-flow from the chemical reaction is conserved and accelerates the reaction rate. The time to maximum reaction rate is loosely equivalent to the time to explosion. This is an extremely conservative calculation and may produce unrealistic times because a fully adiabatic environment is impossible to attain in real life. Hence while this can serve as a bounding limit for safety estimates, it is often an extreme boundary and higher fidelity calculations provide better and more realistic estimates.

ANPZ: TMRad (hrs)					DNDMP: TMRad (hrs)			
Temp (°C)	Isoconv.	ePT (2 peak)	ePT (1 <sup>st</sup> peak only)	ASTM (1 <sup>st</sup> peak only)	Temp (°C)	Isoconv.	ePT	ASTM
250	280.7	81	73.44	17.78	150	305.5	14.48	1.92
275	17.58	6.52	6.12	1.46	170	10.66	3.15	0.43
300	1.52	0.71	0.63	0.15	190	0.99	0.79	0.11

It appears in both cases that the Isoconversional gives the least conservative answer and the ASTM give the most conservative. The isoconversional method is probably the highest fidelity model for this TMRad calculation. The ASTM is the lowest fidelity approach. We have done comparisons of ePT and isoconversional predictions on other materials and had good agreement with experiments in both cases. We have never worked with the ASTM method previously. It is encouraging that the ePT method using

ANPZ produces similar results whether 1 or 2 peaks are used- this supports our advice above to use just the 1<sup>st</sup> peak in calculations if it is impossible to use both.